Three-dimensional imaging and force characterization of multiple trapped particles in low NA counterpropagating optical traps

T. B. Lindballe thue@phys.au.dk
Department of Physics and Astronomy, Science and Technology, Aarhus University, DK-8000 Aarhus C, Denmark

M. V. Kristensen
Interdisciplinary Nanoscience Center, Science and Technology, Aarhus University, DK-8000 Aarhus C, Denmark

A. P. Kylling
Department of Chemistry, Science and Technology, Aarhus University, DK-8000 Aarhus C, Denmark
Unisense FertiliTech A/S, Tueager 1, DK-8200 Aarhus N, Denmark

D. Z. Palima
DTU Fotonik, Department of Photonics Engineering, Technical University of Denmark, DK-2800 Kgs. Lyngby, Denmark

J. Glückstad
DTU Fotonik, Department of Photonics Engineering, Technical University of Denmark, DK-2800 Kgs. Lyngby, Denmark

S. R. Keiding
Department of Chemistry, Aarhus University, DK-8000 Aarhus C, Denmark

H. Stapelfeldt
Department of Chemistry, Aarhus University, DK-8000 Aarhus C, Denmark

An experimental characterization of the three-dimensional (3D) position and force constants, acting on one or multiple trapped polystyrene beads in a weak counterpropagating beams geometry is reported. The 3D position of the trapped particles is tracked by imaging with two synchronized CMOS cameras from two orthogonal views and used to determine the stiffness along all three spatial directions through power spectrum analysis and the equipartition method. For the case of three trapped beads we measure the dependence of the force constants on the counterpropagating beams waist separation. The maximal transverse stiffnesses, is about 0.1 pN/μm per mW at a beam waist separation of 67 μm whereas the longitudinal stiffness is approximately 20 times lower. The experimental findings are in reasonable agreement with a recent physical-geometric optics calculation.
[DOI: http://dx.doi.org/10.2971/jeos.2011.11057]

Keywords: weak optical trap, three-dimensional trapping forces, counterpropagating beams geometry

1 INTRODUCTION

The vast majority of optical trapping schemes, and applications thereof, rely on the use of a single tightly focused laser beam, known as the optical tweezers. Optical trapping can, however, also be accomplished by two counterpropagating laser beams, reported as early as in 1970 by Ashkin in the first experimental demonstration of the ability of light to three- dimensionally (3D) trap a small particle [1]. Some of the advantages of traps based on counterpropagating beams (CB) are large trapping volumes [2, 3], the ability to trap particles with high refractive index (or large particles) [4], and side-ways (i.e. perpendicular to the trapping beam axis) access to the probing and monitoring of the trapped particles. Counterpropagating beams geometries are also well suited for creating multiple optical traps [4, 5, 6, 7, 8].

Quantitative use of optical traps is intimately related to accurate characterization of the position and forces acting on the trapped particles. Unlike the case of single beam optical tweezers accurate measurements of position and trapping forces have been only sparsely reported for CB traps [4, 9]. The purpose of the present manuscript is to provide an experimental 3D characterization of the stiffness of our recently constructed CB trapping station. This is motivated by the fact that sensitive and precise experimental 3D force measurements will be needed, for instance, to discriminate between different models of biological phenomena in life sciences or when exploring possible beamshaping strategies for enhancing the trapping force. Our trapping station employs multiple controllable counterpropagating beams and can, therefore, be used to hold a plurality of particles [7, 8]. In the case of force measurements involving multiple trapped objects it is necessary to characterize the dependence of the trap stiffness on the spatial location in the trapped volume. Here we achieve this goal by simultaneously measuring the force constant for each particle trapped. The force characterization relies on our ability to watch the trapped particles in both end-view (along the trapping beam axis) and in side-view (perpendicular to the trapping beam axis) at the same time by using two synchronized CMOS cameras. This allows us to obtain the stiffness of the trap(s), along all three orthogonal axes in space, by the standard methods of power spectrum analysis and equipartition. Furthermore, the synchronicity of the cameras allow us

Received September 21, 2011; published December 15, 2011

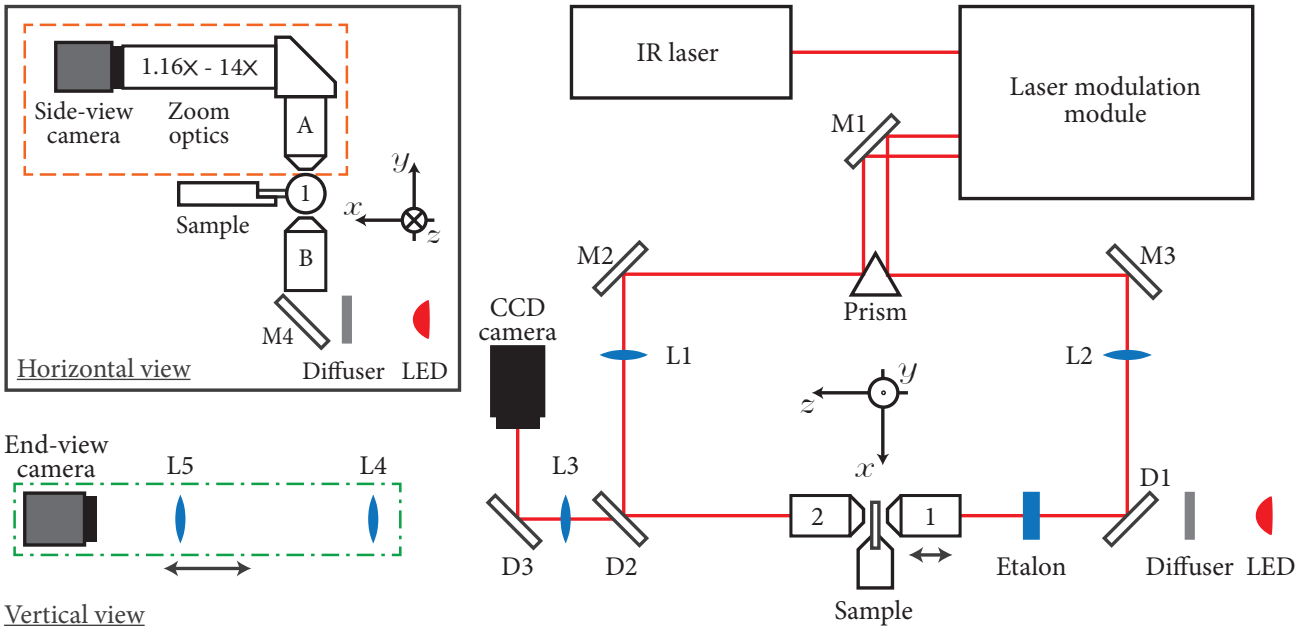

FIG. 1 Schematics of the experimental setup in the vertical view showing the IR fiber laser, the spatial beam modulation module, the optics for the counterpropagating geometry and the end-view imaging unit. The optical trapping occurs in the sample cuvette between objective 1 and 2. The inset (horizontal view) illustrates the side-view imaging unit enabled by the objectives A and B in a vertical arrangement. Objective 1 and the sample cuvette are both mounted on motorized stages. The end-view imaging optics and camera (green dash-dotted box) are mounted on a one-dimensional translation stage while the side-view imaging optics and camera (orange dashed box) are mounted on a three-dimensional translation stage. Nomenclature: M - mirror, D - dichroic mirror, L - lens, LED - light emitting diode.

to make temporal studies of trapped objects in 3D. We introduce our setup and method with a single trapped polystyrene particle and generalize to multiple trapped particles. In the latter case, we also measure the stiffness as a function of the beam waist separation of the counterpropagating beams. This dependence has been the subject of several theoretical studies [10, 11, 12, 13] but to our knowledge it has never been reported experimentally.

2 EXPERIMENTAL SETUP

In our horizontal version of the Biophotonic Workstation (BWS) (Figure 1) [8] we use the unpolarized TEM_{00} mode of an infrared fiber laser (IPG, YLM-20-SC, 20 Watt cw, 1065.5 nm) for trapping. The output of the laser is directed into the laser modulation module (MM) which prepares the beam using a generalized phase contrast (GPC) technique and modulates it using a spatial light modulator (SLM). The SLM can be addressed by a computer and used to specify the number, the size, the shape, the intensity and the spatial position of the laser beams emerging from the MM. The LabVIEW based software addresses one half of the SLM to produce the desired beam configuration and the other half to produce the mirrored configuration. The two sets of beams are relayed via a gold-coated prism to two objectives (1 and 2) sitting opposite to each other. The two objectives (both: Olympus LMPlan IR 50x, 0.55NA) have a working distance of 6 mm and are separated by ∼12 mm when their focal planes are overlapped. During measurements this distance is increased by ∼2 mm due to refraction of the beams on the surface of the rectangular sample cuvette (Hellma Analytics 131-050-40, outer dim.: 20.3×4.2×4.2 mm^3, inner dim.: 20.3×0.25×0.25 mm^3, $n_{1065nm} = 1.450$ at 20° C).

Just before the objectives dichroic mirrors (D1 and D2) are used to enable illumination (LedEngin, Inc., 10W LED, 625 nm) and imaging of the trapped particles. A third dichroic mirror (D3) reflects the residual image of the laser configuration onto the CCD camera (Pulnix TM-1327 GE, 30 fps at 1392×1040 pixels) while the visible image of the trapped particles are transmitted and imaged onto the CMOS of the end-view camera (Photonfocus MV1-D1312-240-CL-8, 170 fps at 1248×1082 pixels, pixel size 8×8 μm^2). The CCD camera supplies a video feed for the LabVIEW program used to address the SLM. The end-view camera monitors the (x, y)-plane of the trapped particles. Furthermore, we introduce the side-view camera (identical to the end-view camera and synchronized to it within 17 nanoseconds) which monitors the (x, z)-plane of the trapped particles (see the inset of Figure 1). The end- and side-view cameras share one common axis and by comparing the plots of two x-tracks, x_{end} and x_{side}, simultaneously observed by the cameras, we verified that the cameras are synchronous. The use of zoom optics (Navitar, 12× UltraZoom with 2.0× standard adapter) in front of the side-view camera enables a large field of view and simplifies positioning of the sample. Both of the CMOS cameras are connected to the same dedicated computer with 2×3 500 GB hard drives arranged in a RAID-0 configuration to accommodate high data acquisition rates (<460 MB/s for the current setup). Videos are saved as 8-bit grayscale *.seq* files which is the standard format of the acquisition software used (NorPix, StreamPix 5).

The particle positions are obtained through post processing of the captured image files. Our tracking algorithm finds the particle by template matching with a Gaussian. It identifies the highest intensity peaks over a given minimum threshold as

particle centers and uses a neighborhood-suppression method to ensure that each particle produces only one peak. To obtain sub-pixel accuracy the positions are refined with a centroid calculation [14]. The computational sub-pixel resolution was estimated by measuring the distance between two stuck particles, which produced a Gaussian distribution with a FWHM of ∼5 nm.

Inside the sample cuvette, at the focal plane of the objectives, each beam has a disc-shaped top hat intensity profile with the same size as the trapped particle. This imitation of a circular aperture makes each beam diffract into an Airy disc pattern [12]. To achieve stable longitudinal trapping objective 1 is displaced away from objective 2, i.e. the disc separation (DS) is increased. Trapping is realized when the scattering forces of the two counterpropagating beams cancel out and the particle is positioned approximately midway between the two discs. A specific DS is set by overlapping the two discs and then displacing objective 1 a distance DS/n_m using a motorized stage. Here we suspend the particles in water so $n_m = 1.33$. Overlapping of the discs is monitored by the CCD camera which images the focal plane of objective 2 and, thus, the position of the stationary disc.

The lenses L4 and L5 (f = 200 mm) and the end-view camera are mounted on a 92 cm-long translation stage (Newport PRL-36). This enables the imaging system as a whole to be displaced out of the initial 4f configuration and up to 30 cm toward the sample. In this way the focus of the end-view camera can be shifted ∼100 microns into the sample away from the focal plane of objective 2. This distance can be increased by using lenses with longer focal lengths. The ability to shift the focus is used to study the dependence of the trap stiffness on the DS (see Sec. 3).

The pixel to micron calibration of the cameras is obtained by tracking a particle sticking to the cuvette wall and moving this using a micrometer screw. In the end-view we get 160 ± 5 nm/pixel and in the side-view we get 169 ± 5 nm/pixel.

To turn off any coherent behavior of the CB we insert a thick etalon (12.7 mm fused quartz) just before objective 1 (Figure 1).

3 RESULTS

3.1 Position and trap stiffness measurements for a single polystyrene bead

First we discuss 3D position tracking and subsequent stiffness determination for a single trapped particle. Figure 2(a1-a3) displays the x, y, and z position of a 10 μm diameter polystyrene bead over a time interval of 15 min. The 3D position, recorded every 10 ms, was determined by postprocessing the captured *.seq* files.

To avoid correction of the friction coefficient, γ, due to influence from the cuvette walls [15] we initially aligned the trapping beams such that the bead was located approximately in the middle of the cuvette, i.e. about 125 μm from each side wall and several millimeters from each end of the channel. The disc separation was set to 67 μm, which is close to the value where the transversal stiffness is maximized (see Sec. 3.2). The y-position (see Figure 1) is recorded with the end-view camera and the z-position is recorded with the side-view camera. For the x-position both cameras can be used. Here, we only present results of the x-position using the end-view camera but we note that measurements performed with the side-view camera give identical results for the force analysis discussed below. The synchronous observation of all three axes make the characterization of the optical traps straightforward and direct. In the current setup we directly measure the three spatial coordinates of the trapped particle and, thus, it is not necessary to calibrate the position of the trapped particle, e.g. through the light intensity of the particle imaged at the end-view camera.

Next, the stiffness of the trap is determined. Two standard methods, equipartition and power spectrum [16], both using the position measurements, were applied. In Figure 2(b1-b3) the histograms of the particle positions are shown for the three orthogonal directions and they form the basis for the equipartition method [16]. Each distribution in the three panels can be well fit with a Gaussian (red curve). According to Wong and Halvorsen the variance, σ^2_{meas}, in the Gaussian fit-expression has to take into account the motion blur arising from a finite exposure time, $W = 1.5$ ms, of the camera [17]. The blur correction is defined in terms of $\alpha = W/\tau$, the ratio between the exposure time W and the particle relaxation time $\tau = \gamma/\kappa$. In our case the trap is weak which make $\alpha < 1$ and the correction is well determined by the first few orders of the expression given in [17]. Thus, we can write the blur-corrected variance as

$$\sigma^2_{\text{meas}} = \frac{k_B T}{\kappa}\left(1 - \frac{\alpha}{3} + \frac{\alpha^2}{12}\right), \tag{1}$$

which is included in the Gaussian fits in Figure 2. The stiffness is obtained directly from the fits: $\kappa_x = 1.14 \pm 0.009$ pN/μm, $\kappa_y = 0.887 \pm 0.0062$ pN/μm, $\kappa_z = 0.0526 \pm 0.00054$ pN/μm. The uncertainties was obtained from the fit as the confidence interval (one standard deviation) of the fitted parameter. We note that the laser power used for trapping is 11.6 mW, which means that the power-normalized stiffness are 0.098, 0.076 and 0.0045 pN/μm per mW in the x, y, and z direction, respectively.

To obtain the power spectra we followed the standard procedure of Fourier transforming and norm squaring the particle position traces and divided this by the total acquisition time. The results are displayed in Figure 2(c1-c3). We obtain the stiffness from the corner frequency, $f_c = \kappa D/2\pi k_B T$, and the diffusion constant, D. These two parameters are determined by fitting the power spectral density of the position measurement with the theoretical power spectrum (red curves)

$$P(f, f_c, D) = \sum_{n=-3}^{3} \frac{D}{2\pi^2 (f_n^2 + f_c^2)} \text{sinc}\,(W f_n)^2, \tag{2}$$

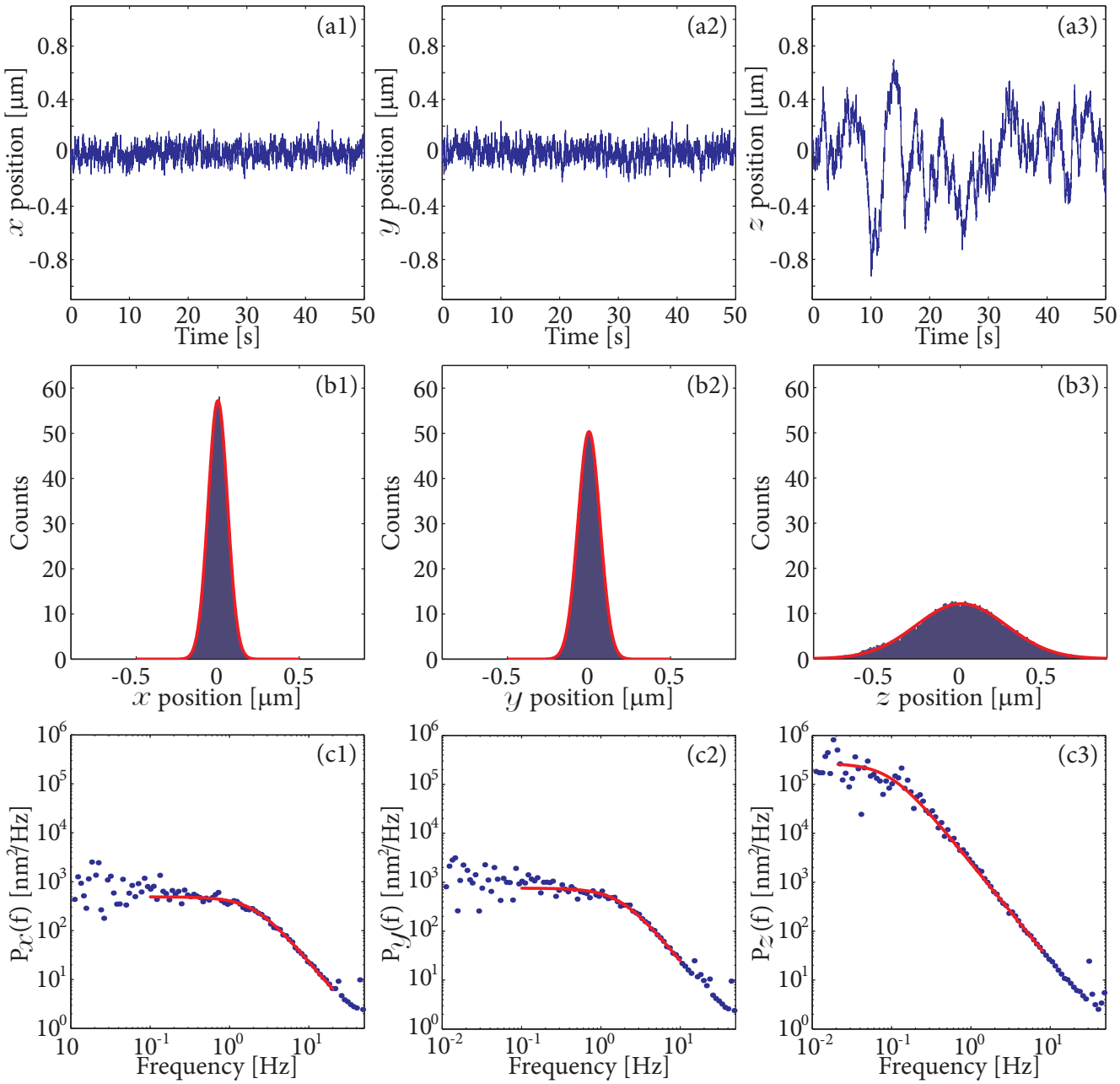

FIG. 2 Panel (a1-a3): The first 50 seconds of the x-, y- and z-position measurements of a single 10 μm diameter trapped polystyrene bead. Panel (b1-b3): Histograms of the particle position traces and Gaussian fits (red curves). Panel (c1-c3): Power spectra of the particle position traces. The red curves represent fits to the data points (see text) and the lengths of the curves indicate the frequency range used in the fits.

including the corrections for motion blur through the sinc-term and for aliasing through $f_n = f + nf_{sample}$ for $|n| \leq 3$, where f is the measured frequency and $f_{sample} = 100$ Hz is the sampling frequency of the camera [18, 19]. Following the central limit theorem it is custom to block data points on the logarithmic scale before fitting, i.e. to average over exponentially growing frequency intervals, to obtain Gaussian distributed data values from an ensemble of the true exponentially distributed data points [19]. This allows for a standard least squares fitting. Our frequency resolution, however, is not good enough that we can obtain Gaussian distributed data points in the low end of the spectrum. Therefore, we make a maximum likelihood estimation on the raw, non-averaged data and maximize the probability of getting the measured power spectrum, $P^{(meas)}(f)$, with N exponentially distributed data points from the model $P(f, f_c, D)$ in Eq. (2) given the parameters f_c and D,

$$\max\left\{\prod_{i=1}^{N}\left[\frac{1}{P(f,f_c,D)}\exp\left(\frac{P^{(meas)}}{P(f,f_c,D)}\right)\right]\right\}. \qquad (3)$$

For numerical reasons this problem is rephrased to that of minimizing the negative logarithm of Eq. (3). We obtain $f_{c,x} = 2.19 \pm 0.014$ Hz and $\kappa_x = 1.20 \pm 0.004$ pN/μm, $f_{c,y} = 1.82 \pm 0.015$ Hz and $\kappa_y = 0.935 \pm 0.0054$ pN/μm, $f_{c,z} = 0.096 \pm 0.0028$ Hz and $\kappa_z = 0.0498 \pm 0.00148$ pN/μm. As seen the values agree well with those obtained from the equipartition method, $\kappa_{\text{power}}/\kappa_{\text{equi}} = 1.05$ for the x and y results. If the axial stiffness of the trap is reduced it becomes difficult to accurately determine a corner frequency due to very few data points in the pertinent low frequency part of the spectrum. In

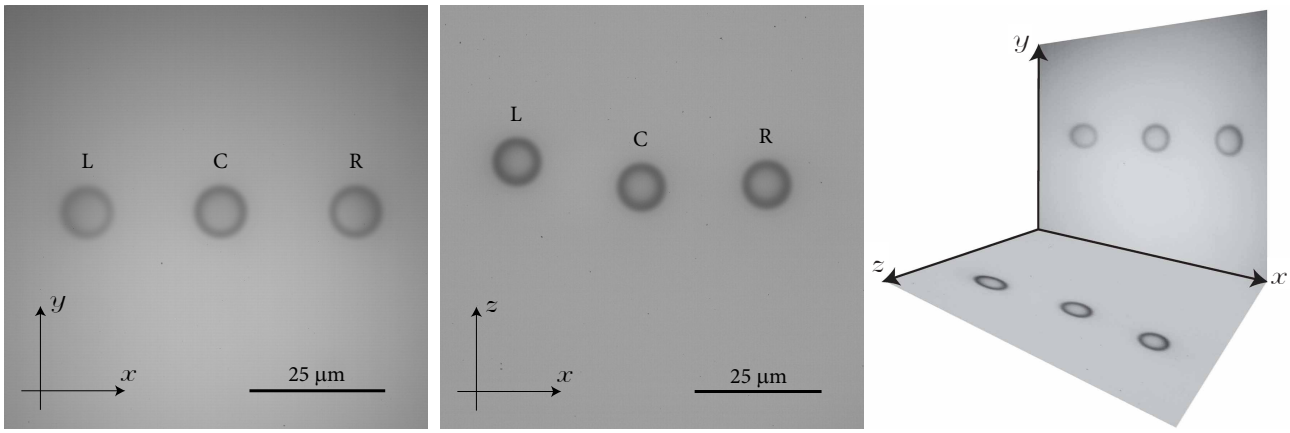

FIG. 3 Images of three 10 μm polystyrene beads trapped in a near-linear configuration. The end-view (left) provides an image of the x,y plane and the side-view (middle) an image of the x,z plane. To the right the two images have been placed to illustrate the real geometry of the setup. The disc separation was 67 μm.

principle, this could be overcome by tracing the particle for very long times which is, however, practically difficult. Therefore, we use the equipartition method to provide reliable determinations of the very weak z-trapping.

3.2 Position and trap stiffness measurements for multiple trapped particles

To illustrate the ability to characterize multiple particles at the same time we conducted measurements on three simultaneously trapped polystyrene beads. The beads have a diameter of 10 μm and they are held in a near-linear formation with a spacing of 25 μm. At each sampling time we recorded an image with both the side-view and the end-view camera and determined the center of each of the three beads. Examples of images are displayed in Figure 3 illustrating the near-linear trapping geometry. Hereafter, the force constants were determined by the equipartition and the power spectrum methods. The measurements were carried out for a number of disc separations ranging from 0 to 300 μm. In practice, the disc profiles of the two CB are overlapped and then, by moving objective 1 (Figure 1), one beam is displaced a specific DS distance along the propagation direction of the other beam. The results for the x-, y-, and z-components of the stiffness for each of the three particles are displayed in Figure 4. Each point on the graph in a) and b) represents the result of a power spectrum analysis performed on a 15 min long 100 Hz movie whereas the data points in graph c) were obtained from a equipartition analysis of the same amount of data.

Focusing first on the x- and the y-components we note that in common for the three beads the highest stiffness is attained for a disc separation around 60-100 μm. At larger disc separations the stiffness decreases essentially monotonically. These observations are in fair agreement with calculations of the transverse stiffness as a function of DS [12]. Based on the simulated stiffness qualities given in [12] (region III of Fig. 4 in that work), $Q_y/\Delta y = 10 \cdot 10^{-3}$ μm^{-1} and $Q_z/\Delta z = 1.5 \cdot 10^{-3}$ μm^{-1}, we get the calculated trap stiffnesses: $\kappa_x^{\mathrm{calc}} = \kappa_y^{\mathrm{calc}} = 2.06$ pN/μm and $\kappa_z^{\mathrm{calc}} = 0.15$ pN/μm. Again, this is in reasonable agreement with the experimental findings. In that work it was assumed that a 10 μm diameter particle was trapped precisely in the center between two counterpropagating top-hat beams. As we discuss below deviations from this simplified picture may occur.

Figure 4(b) shows that along the y-direction the force constant is almost the same for the three beads at all disc separations. This is reasonable given the fact that the y- coordinates are the same and the z-coordinates almost the same for the three particles. By contrast, the dependence of κ_x on DS for the three beads differ more, see Figure 4(a). This is to be expected since it is along the x-direction that the particles are separated and because the optical axis of the optical system preceding the SLM is centered on the SLM. This give rise to larger aberrations of the R-trap than the L-trap, which is the closest to the SLM center, and make the traps x-characteristics slightly different.

Finally, κ_z has a more structured dependence on DS (Figure 4(c) with several distinct local maxima and minima. In the model by Palima *et. al.* [12], where it is assumed that the particle position remains exactly midway between the two beam discs, there are DS regions where stable trapping does not occur. In practice the particle will move away from the center of the unstable trap to a position where stable axial trapping is possible rather than being pushed out of the trap along the trapping axis as would be the consequence of the modeling. We indirectly observed the existence of stable z-positions as a change in the relative z-positioning of the three particles. The straight line configuration seen in the side-view thus was not equally straight at all disc separations.

4 CONCLUDING REMARKS

In conclusion, we have shown that the use of two synchronized cameras, viewing the trapped particles from two orthogonal directions, makes it possible to 3D track the position of one or several particles. The position measurements were used to quantitatively determine, for the first time, the force constants for disc-shaped CB traps along all three spatial directions. This was done both for a single trapped particle and for three simultaneously trapped particles. Furthermore,

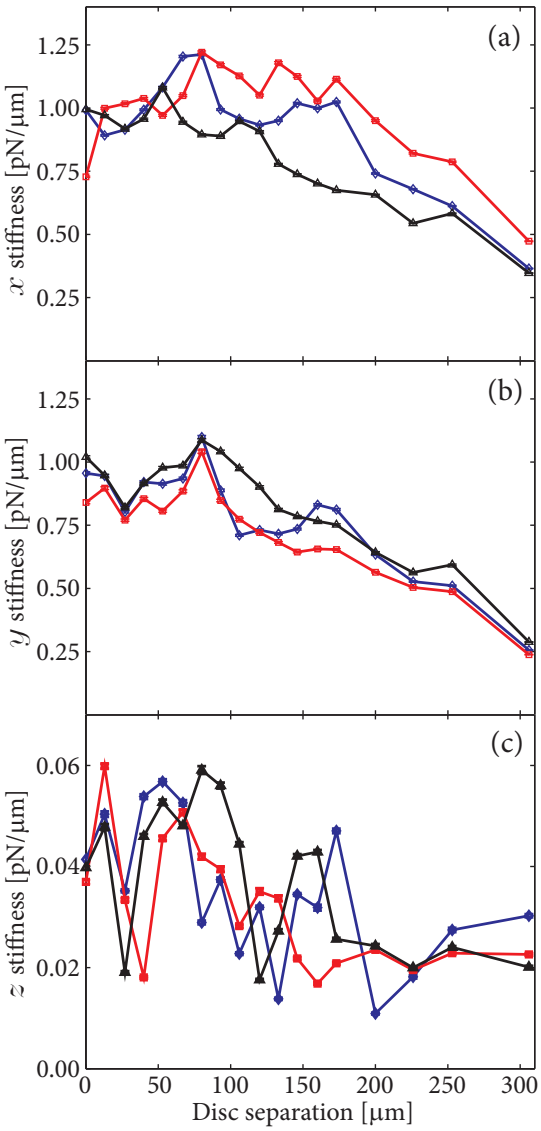

FIG. 4 The trap stiffness experienced by three trapped particles, in a linear trap geometry (see Figure 3), as a function of disc separation for (a) the x-, (b) the y-, and (c) the z-axis. Data for both the left, L (red squares), the center, C (blue diamonds), and the right, R (black triangles), particle are shown.

we have, to our knowledge, conducted the first experimental study of the influence of disc separation on the force constants in a CB geometry. The transversal stiffness, i.e. the κ_x and the κ_y results, agree reasonably with the hybrid physical–geometric optics calculations by Palima *et al.* [12] and verifies the existence of stable trapping at lower disc separations (as opposed to far-field conventional spacing). This enables stiffer traps than achieved in the conventional far-field geometry and minimizes aberrations as the microscope objectives may not be aberration-corrected when imaging far from the focal plane. Having found stiffer traps in regions where the beams are "less Gaussian looking", it will be interesting to search for optimal light shapes for improving trap stiffness further. The comparison of the experimental axial stiffness (κ_z results) with calculations are more subtle. We observed that the particles relax into "off-centered" equilibrium positions which accounts for the fact that 3D trapping is realized at all disc separations including the regions found to be unstable by theory. Experiment and theory does, however, agree on the z-stiffness being highly sensitive to the disc separation.

Our work is in line with a strong current interest for 3D position and force characterization of trapped objects employing, for instance, holographic microscopy [20, 21] and stereoscopic imaging [22]. The lateral force constants reached in the present work are on the order of 1 pN/μm and the axial stiffness about a factor of 20 smaller. By comparison to most single beam tweezers this is a weak trap. This may be an advantage in certain cases, for instance, when studying weak interaction potentials. If needed the current CB setup can, however, be adjusted to increase the force constants by an order of magnitude or more, by employing higher laser powers and/or by adjusting the beam modulation module, while preserving the ability to view the object in both end-view and side-view. Alternatively, position stabilization can be implemented [9, 23]. From a force analysis point-of-view stiffer traps provide the advantage of a much reduced acquisition time needed for data accumulation.

The present experimental results were obtained by CMOS cameras running at a repetition rate of 100 Hz. By lowering the region of interest the sampling frequency can be increased (>600 Hz for the current cameras) and thus allow for the determination of force constants for stronger traps. In addition, it has been demonstrated that cameras running at 10 kHz are applicable for determining the position of trapped particles [24]. Implementation of such cameras will allow our method for 3D position tracking to also work for multiple particles trapped by much stronger forces than reported here.

An application of the CB traps is trapping of large and possibly irregularly shaped particles, where 3D monitoring of the position and orientation of the particles could be highly useful. Preliminary studies were carried out showing that the setup easily holds and manipulates polystyrene beads as big as 30 μm in diameter. In addition, we demonstrated that a protein crystal of similar size could be moved and rotated, an ability that potentially could be used in crystallography [25, 26].

5 ACKNOWLEDGEMENTS

This work is supported by the Danish Technical Scientific Research Council (FTP) and the Siemens Foundation. We acknowledge discussions with Søren Gammelmark on the fitting algorithm for the Power Spectrum analysis and Sandeep Tauro for preparing the GPC section of the modulation module.

References

[1] A. Ashkin, "Acceleration and trapping of particles by radiation pressure" Phys. Rev. Lett. **24**, 156 (1970).

[2] A. Constable, J. Kim, J. Mervis, F. Zarinetchi, and M. Prentiss, "Demonstration of a fiberoptic light-force trap" Opt. Lett. **18**, 1867–1869 (1993).

[3] M. Pitzek, R. Steiger, G. Thalhammer, S. Bernet, and M. Ritsch-Marte, "Optical mirror trap with a large field of view" Opt. Express **17**, 19414–19423 (2009).

[4] A. van der Horst, P. D. J. van Oostrum, A. Moroz, A. van Blaaderen, and M. Dogterom, "High trapping forces for high-refractive index

particles trapped in dynamic arrays of counterpropagating optical tweezers" Appl. Opt. **47**, 3196–3202 (2008).

[5] P. J. Rodrigo, V. R. Daria, and J. Glückstad, "Real-time three-dimensional optical micromanipulation of multiple particles and living cells" Opt. Lett. **29**, 2270–2272 (2004).

[6] I. R. Perch-Nielsen, P. J. Rodrigo, and J. Glückstad, "Real-time interactive 3D manipulation of particles viewed in two orthogonal observation planes" Opt. Express **13**, 2852–2857 (2005).

[7] P. J. Rodrigo, I. R. Perch-Nielsen, C. A. Alonzo, and J. Glückstad, "GPC-based optical micromanipulation in 3D real-time using a single spatial light modulator" Opt. Express **14**, 13107–13112 (2006).

[8] H.-U. Ulriksen, J. Thøgersen, S. R. Keiding, I. R. Perch-Nielsen, J. S. Dam, D. Z. Palima, H. Stapelfeldt, and J. Glückstad, "Independent trapping, manipulation and characterization by an all-optical biophotonics workstation" J. Eur. Opt. Soc-Rapid **3**, 08034 (2008).

[9] R. Bowman, A. Jesacher, G. Thalhammer, G. Gibson, M. Ritsch-Marte, and M. Padgett, "Position clamping in a holographic counterpropagating optical trap" Opt. Express **19**, 9908–9914 (2011).

[10] P. J. Rodrigo, I. R. Perch-Nielsen, and J. Glückstad, "Three-dimensional forces in GPC-based counterpropagating-beam traps" Opt. Express **14**, 5812–5822 (2006).

[11] H. Sosa-Martinez and J. C. Gutierrez-Vega, "Optical forces on a Mie spheroidal particle arbitrarily oriented in a counterpropagating trap" J. Opt. Soc. Am. B **26**, 2109–2116 (2009).

[12] D. Z. Palima, T. B. Lindballe, M. V. Kristensen, S. Tauro, H. Stapelfeldt, S. R. Keiding, and J. Glückstad, "Alternative modes for optical trapping and manipulation using counter-propagating shaped beams" J. Opt. **13**, 044013 (2011).

[13] E. Sidick, S. Collins, and A. Knoesen, "Trapping forces in a multiple-beam fiber-optic trap" Appl. Opt. **36**, 6423–6433 (1997).

[14] S. C. Chapin, V. Germain, and E. R. Dufresne, "Automated trapping, assembly, and sorting with holographic optical tweezers" Opt. Express **14**, 13095–13100 (2006).

[15] F. Gittes and C. F. Schmidt, "Thermal noise limitations on micromechanical experiments" Eur. Biophys. J. **27**, 75–81 (1998).

[16] K. C. Neuman and S. M. Block, "Optical trapping" Rev. Sci. Instrum. **75**, 2787–2809 (2004).

[17] W. P. Wong and K. Halvorsen, "The effect of integration time on fluctuation measurements: calibrating an optical trap in the presence of motion blur" Opt. Express **14**, 12517–12531 (2006).

[18] A. van der Horst and N. R. Forde, "Power spectral analysis for optical trap stiffness calibration from high-speed camera position detection with limited bandwidth" Opt. Express **18**, 7670–7677 (2010).

[19] K. Berg-Sørensen and H. Flyvbjerg, "Power spectrum analysis for optical tweezers" Rev. Sci. Instrum. **75**, 594–612 (2004).

[20] S.-H. Lee and D. G. Grier, "Holographic microscopy of holographically trapped three-dimensional structures" Opt. Express **15**, 1505 (2007).

[21] F. C. Cheong, B. J. Krishnatreya, and D. G. Grier, "Strategies for three-dimensional particle tracking with holographic video microscopy" Opt. Express **18**, 13563 (2010).

[22] R. Bowman, D. Preece, G. Gibson, and M. Padgett, "Stereoscopic particle tracking for 3D touch, vision and closed-loop control in optical tweezers" J. Opt. **13**, 044003 (2011).

[23] S. Tauro, A. Banas, D. Z. Palima, and J. Glückstad, "Dynamic axial stabilization of counter-propagating beam-traps with feedback control" Opt. Express **18**, 18217–18222 (2010).

[24] O. Otto, F. Czerwinski, J. L. Gornall, G. Stober, L. B. Oddershede, R. Seidel, and U. F. Keyser, "Real-time particle tracking at 10,000 fps using optical fiber illumination" Opt. Express **18**, 22722 (2010).

[25] P. A. Bancel, V. B. Cajipe, and F. Rodier, "Manipulating crystals with light" J. Cryst. Growth **196**, 685–690 (1999).

[26] W. Singer, H. Rubinsztein-Dunlop, and U. Gibson, "Manipulation and growth of birefringent protein crystals in optical tweezers", Opt. Express **12**, 6440–6445 (2004).